

Effect of interdot magnetostatic interaction on magnetization reversal in circular dot arraysV. Novosad,^{1,2,*} K. Yu. Guslienko,³ H. Shima,^{2,4} Y. Otani,^{2,4} S. G. Kim,² K. Fukamichi,² N. Kikuchi,⁵ O. Kitakami,⁵ and Y. Shimada⁵¹*Materials Science Division, Argonne National Laboratory, Argonne, Illinois 60439*²*Department of Materials Science, Graduate School of Engineering, Tohoku University, Sendai 980-8579, Japan*³*School of Physics, Korea Institute for Advanced Study, Seoul 130-012, Korea*⁴*Japan Science & Technology Corporation, CREST, Kawaguchi 3320012, Japan*⁵*Institute of Multidisciplinary Research for Advanced Materials, Tohoku University, Sendai 980-8577, Japan*

(Received 23 July 2001; published 3 January 2002)

The effect of the interdot magnetostatic interaction on the magnetization reversal due to the “nucleation” and “annihilation” of magnetic vortices in arrays of ferromagnetic submicron circular dots has been investigated experimentally and theoretically. The magnetostatic interaction plays an important role in magnetization reversal for the arrays with a small interdot distance, leading to decreases in the vortex nucleation and annihilation fields, and an increase in initial susceptibility.

DOI: 10.1103/PhysRevB.65.060402

PACS number(s): 75.75.+a, 75.30.Gw, 75.60.Jk

The array of identical magnetic particles (dots), whose geometry, size, and interdot spacing can be precisely controlled during the microfabrication process, is a model system well suited for a direct comparison of theoretical prediction and experimental data. Magnetization reversal in the dot arrays is initiated in accordance with the balance of magnetostatic, exchange, and magnetic anisotropy energies when the interdot coupling is negligible. The magnetostatic interaction should be taken into account to describe the magnetic state of the patterned film, when interdot spacing is less than the lateral dot size. The dot shapes (circular or elliptical cylinder or rectangular prism, usually) are an important factor for coupling calculations in such close-packed dot arrays.

Assuming small dot thickness of a few tens of nm, the magnetic state of the dots as a function of the dot in-plane size can be single domain, vortex type (for magnetically soft or polycrystalline dots) or closure-flux state (for epitaxial dots). For single-domain dot arrays the effect of magnetostatic coupling was studied experimentally^{1–3} and theoretically.⁴ A ferromagnetic dot demonstrates nonuniform remanent magnetization distribution when its in-plane dimensions are larger than the exchange length (~ 10 nm), but not large enough to form domain structure. An example of such a nonuniform magnetic state is a “vortex” structure that can be realized in magnetically soft flat dots with submicron sizes.^{5,6} The magnetic vortices have been directly observed by Lorenz electron microscopy⁷ and magnetic force microscopy (MFM).^{8–10} Besides fundamental physical interests, circular dot and ring-type nanostructures are possible candidates for magnetic memory cells.^{11,12} As far as we know, there are no experimental data available on the interdot magnetostatic interaction in dot arrays with nonuniform remanent state. Experiments related to magnetization reversal of the magnetic vortex states were conducted only for arrays of well-separated dots, i.e., when the interdot magnetostatic interaction is negligibly small. Moreover, the fact that the closure of the magnetic flux structure is realized in ferromagnetic dots with vortex-type spin distribution has led some researchers^{13–15} to a not correct assumption that the dots are

not magnetostatically coupled in the applied magnetic field, even for high-density packing of the dots.

In this paper we report the experimental and theoretical studies of the magnetization reversal due to the “nucleation” and “annihilation” of magnetic vortices in arrays of ferromagnetic submicron circular dots with variable diameter and the interdot distance. It will be demonstrated below that the magnetostatic interdot interaction has a strong destabilizing effect on the vortex magnetic state. The experimental data and calculations show that vortex nucleation and annihilation fields are strongly dependent on the interdot distance.

Samples of circular dot arrays were fabricated on a silicon wafer using electron beam (EB) lithography and lift-off techniques. A double layered resist spin coating and highly directional EB evaporation were used to obtain circular dots with sharp edges. The bottom layer is more sensitive to an electron beam than the top layer, therefore, and forms an undercut profile when developed. This facilitates a lift-off process. Although EB lithography is a relatively slow process, this technique is very convenient to fabricate arrays of submicron dots with different diameters and periods, within a limited area of substrate. Consequently, identical properties of magnetic material, such as grain size, distribution, and orientation, and film thickness may be obtained over the whole sample. The magnetic film was deposited on a water-cooled substrate from a permalloy ($\text{Fe}_{81}\text{Ni}_{19}$) target. The growth ratio was of ~ 1 Å/s. The as-deposited polycrystalline reference film shows a coercive field of about 2 Oe and uniaxial anisotropy field of 8 Oe. We have prepared the arrays with dot radii R of 0.2, 0.3, and 0.4 μm and variable interdot distances, d . Atomic force microscope (AFM) observation shows that the dot thickness L is typically 80 nm and that surface roughness is of ~ 2 nm. The dots were arranged into rectangular lattices. The interdot distance along one axis of the lattice is set to the dot diameter for all the patterned arrays, whereas the distance along the other axis was varied for different arrays, from 30 to 800 nm. Vortex nucleation, annihilation, and initial susceptibility were determined from hysteresis loops, measured using the longitudinal magneto-optical Kerr effect.

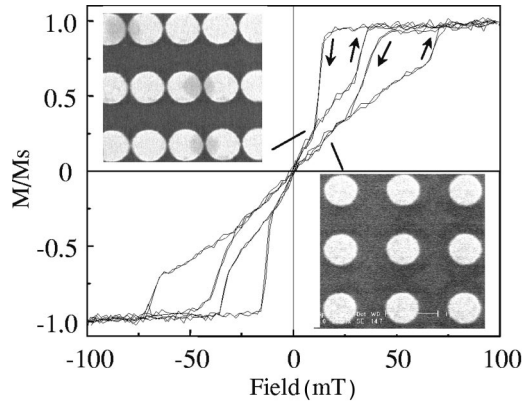


FIG. 1. Hysteresis loops of permalloy dot arrays with diameter $0.8 \mu\text{m}$, thickness 80 nm , and interdot distance 800 and 30 nm . The insets show scanning electron microscope pictures of these arrays.

Figure 1 shows two hysteresis loops for dots with a diameter of $0.6 \mu\text{m}$, but different interdot distances. The field was applied along the horizontal direction. A magneto-optical technique yields information on the magnetization reversal process averaged over many 1000's of dots. Nevertheless, the loops have a clear signature of the magnetization reversal with “nucleation” and “annihilation” of magnetic vortices. With decreasing field from the saturated state, the magnetization gradually decreases, showing an abrupt jump at the nucleation field H_n . In this field a single magnetic vortex is formed inside each dot. When the applied magnetic field is equal to the annihilation field H_{an} , the vortex vanishes and the dot is stabilized in the single-domain state. Zero remanence magnetization is a typical feature of a vortex remanent state in soft ferromagnetic particles with a circular shape. The low-field (linear) part of hysteresis loop is reversible. This part corresponds to vortex displacement from the dot center as whole. The existence of a vortex spin distribution in our samples was confirmed by additional MFM measurements. The vortex formation and displacement in circular dots were discussed in more detail in Refs. 7, 8, 10, 16, and 17. Here we focus our interest on the effect of interdot magnetostatic coupling on the magnetization reversal process.

The magnetization curve of the rectangular array depends on the angle between the external field and the lattice orientation. The easy magnetization axis is parallel to the row of arrays with a small interdot spacing. The hysteresis loops measured along the hard axis are almost identical to those for the arrays of isolated dots with the same geometry.

Figure 2 summarizes the experimental data for nucleation H_n and annihilation H_{an} fields. The changes in H_n and H_{an} with the dot diameter are consistent with published data.^{8,16} For dot arrays with a small diameter the vortex nucleation occurs in a stronger field, and a stronger magnetic field is required to uniformly magnetize the dot. For a very small R , the vortex becomes unstable, and a transition to single-domain (“leaf” or “flower”) state with in-plane or out-of-plane magnetization is expected.⁶ As the dot diameter increases, both nucleation and annihilation fields decrease according to the size-dependent in-plane demagnetizing factor.¹⁷ The values of H_n and H_{an} , and the slope of the

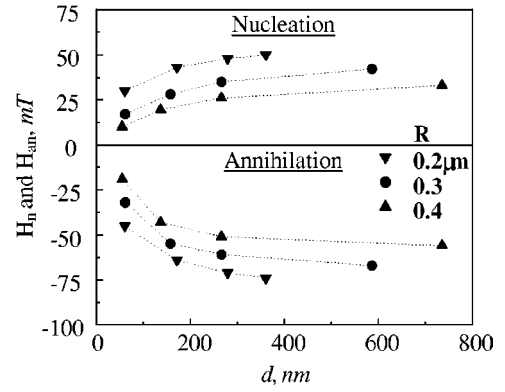


FIG. 2. Experimental nucleation and annihilation fields in the rectangular arrays of permalloy dots as a function of interdot distance d .

linear part of hysteresis loop depend not only on the dot diameter and the thickness, but also on the interdot distance. As seen in Fig. 2, nucleation and annihilation fields decrease, whereas an initial susceptibility of the vortex increases with decreasing interdot distance.

To model the magnetic properties of magnetostatically interacting dots we made following assumptions. First, all dots in an array are identical and have the same vortex type spin distribution in remanence independent of interdot distance. Second, we assumed that the magnetization distribution $\mathbf{M}(\mathbf{r})$ does not depend on coordinate along the dot thickness z (L is about of exchange length). Next, we used a “rigid” vortex model, which assumes that the vortex moves under applied magnetic field while keeping its shape.¹⁷ The total dot magnetic energy consists of (i) magnetostatic energy W_m , (ii) Zeeman energy W_H , and (iii) exchange energy W_{ex} . The magnetostatic energy W_m is influenced by the interdot interaction, especially for close-packed dot arrays with $d/R < 1$, whereas the exchange W_{ex} and Zeeman W_H contributions are single-dot quantities, i.e., they do not depend on the interdot distance. To calculate W_m , we considered a periodical arrangement of the dots in the film plane with the reciprocal lattice vector $\mathbf{k} = (k_x, k_y)$. For the rectangular lattice $(k_x, k_y) = 2\pi(m/T_x, n/T_y)$, where m and n are integers, $T_{x,y} = 2R + d_{x,y}$ are the array periods. We used the general expression for the magnetostatic energy density per unit volume of in-plane magnetized patterned film in Ref. 4, whereby the magnetostatic coupling in two-dimensional arrays of identical cylindrical dots was calculated:

$$W_m = 2\pi \sum_r \sum_k \frac{f(kL)}{k^2} |(\mathbf{k} \cdot \mathbf{M}_k)|^2, \quad (1)$$

where $f(x) = 1 - [1 - \exp(-x)]/x$, $\mathbf{M}_k^\alpha = S^{-1} \int_S d^2\rho \mathbf{M}^\alpha(\rho) \times \exp(i\mathbf{k}\rho)$, $\alpha = x, y$, S is the square of the unit cell of the dot lattice, and ρ is the radial vector in the x - y plane. To calculate the vortex displacement l within the “rigid vortex” model we used the Usov’s magnetization distribution $M^\alpha(\rho)$.¹⁸ The volume magnetic charges are absent and surface face charges are unchanged under the vortex shift within

the model. The increase in energy related to the side surface charges is compensated by a decrease in the exchange and Zeeman energies. For a small vortex displacement $s=l/R$, we could obtain the following decomposition of the magnetostatic energy density (in units of M_s^2 and normalized per unit dot volume):

$$w_m(s) = w_m(0) + 2\pi F(\beta, \delta)s^2 + O(s^4), \quad (2)$$

$$F(\beta; \delta) = \frac{4\pi}{T_x T_y} \sum_{\mathbf{k}} f(\beta k R) \frac{J_1^2(kR)}{k^2} \cos^2(\varphi_{\mathbf{k}} - \varphi_H),$$

where $\delta = d/R$ ($d_x = d$) is the normalized interdot distance, $\beta = L/R$, $J_1(x)$ is the Bessel function, $\varphi_{\mathbf{k}}$ and φ_H are the polar angles of the vectors \mathbf{k} and \mathbf{H} , respectively. The function $F(\beta, \delta)$ leads to uniaxial anisotropy induced by interdot coupling with an easy magnetization axis parallel to the shortest period T_x of the rectangular dot array ($\varphi_H = 0$). The exchange W_m and Zeeman W_H energies are given by Guslienko *et al.*:¹⁷

$$w_{\text{ex}}(s) = w_{\text{ex}}(0) + \frac{1}{2} \left(\frac{R_0}{R} \right)^2 \ln(1 - s^2), \quad (3)$$

$$w_H(s) = -h[s + O(s^3)], \quad (4)$$

where $h = H/M_s$, R_0 is the exchange length (about of 14 nm for FeNi), M_s is the saturation magnetization. By minimizing the sum of all energy contributions one can obtain the equilibrium shift of the vortex center s , as well as other physical parameters of the dot array. We used the decomposition of the energies defined by Eqs. (2)–(4) to rewrite the total energy density in a dimensionless form:

$$\begin{aligned} w(s) &= w_{\text{ex}}(s) + w_m(s) + w_H(s) \\ &= w(0) + a(\beta, \delta, R)s^2 - hs + O(s^4), \end{aligned} \quad (5)$$

with $a(\beta, \delta, R) = 2\pi F(\beta, \delta) - 1/2(R_0/R)^2$.

The vortex state is the ground state at $H=0$ for typical dot parameters, and the coefficient $a(\beta, \delta, R) > 0$. Equation (5) immediately yields an equilibrium displacement s of the vortex center. The initial (anisotropic) magnetic susceptibility of the coupled cylindrical dots for an in-plane field is $\chi_0 = [2a(\beta, \delta, R)]^{-1}$. The vortex annihilation occurs when the vortex core crosses the dot boundary at $s \cong 1$. The first approximation of the vortex annihilation field H_{an} can be obtained extrapolating the linear part of $M(H)$ dependence up to the magnetization saturation M_s [$M(H_{\text{an}}) = \chi_{\text{int}} H_{\text{an}} = M_s$, $s \cong 1$] and is determined by the following expression:

$$H_{\text{an}}(\beta, \delta, R) = 2a(\beta, \delta, R)M_s. \quad (6)$$

The intradot magnetostatic interaction gives a positive and the intradot exchange interaction and the interdot magnetostatic coupling (through induced stray fields) give negative contributions to the dot annihilation field. A model of the vortex nucleation field in dot arrays with nonuniform remanent magnetization distribution will be considered separately in Ref. 19.

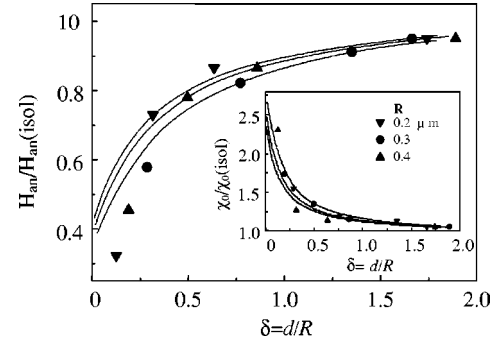


FIG. 3. Normalized annihilation fields determined by the experiment (markers) and the calculation (lines) vs the normalized interdot distance δ . The inset shows scaled initial susceptibility, as determined from the analytical calculation and hysteresis loops.

Figure 3 shows experimental results and calculations using Eq. (6) for the annihilation field as a function of the reduced interdot distance $\delta = d/R$. The magnetic field is applied along the shortest unit cell period. The value of H_{an} are the same as shown in Fig. 2, but normalized to the annihilation field of isolated dots. This allows one to compare the effect of interdot coupling in dot arrays with the different R and d . The inset in Fig. 3 compares the normalized initial susceptibility $\chi_0/\chi_0(\text{isol})$ as calculated using the above mentioned analytical expression and experimentally determined from the magneto-optical hysteresis loops. The modeling is in good agreement with the experimental data, whereby the influence of interdot interaction is appreciable for $d < R$. The samples with smaller interdot distances shows higher initial susceptibility. This means that the dot arrays with strong interdot magnetostatic coupling have higher mobility of the vortex core than an isolated dot with the same sizes.

The experimental results and calculations show for the same δ that the effect of magnetostatic coupling is weaker for dots with a larger diameter (i.e., for smaller dot aspect ratio L/R). However, the difference is small, and then, the interdot distance normalized to dot radius can be used as a key parameter to determine the strength of the interdot coupling effect, as supported by the scaled vortex nucleation fields (Fig. 4). The values of H_n and H_{an} decrease almost two times for the arrays with the smallest interdot distances in comparison to isolated dots.

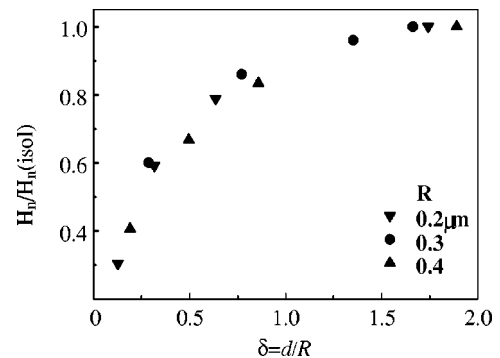


FIG. 4. The normalized experimental nucleation fields vs the normalized interdot distance δ .

In the absence of an external magnetic field, the magnetically soft dots are in a magnetization curling state. The centers of the vortices are located at the centers of the dots, and the reduced vortex core radius is small, so that magnetic charges are practically absent and the magnetostatic interaction of the dots is negligible as stated in Refs. 10 and 15, even for distances d close to zero. In an external magnetic field, the centers of the vortices are shifted, resulting in a nonzero dot dipolar moment $\langle \mathbf{M} \rangle$ and appearance of interdot magnetostatic coupling. A nonzero quadrupolar and high-order multipole moments of the in-dot magnetization distribution leads to an induced magnetic fourfold anisotropy, even for a square dot array.²⁰ For considered rectangular arrays, $\langle \mathbf{M} \rangle \neq 0$ results in uniaxial anisotropy and the in-dot quadrupolar moments are not so important due to dominant interdot dipolar coupling. The experimental study of hysteresis loops of close-packed dot arrays with different lattice symmetry is in progress.

In summary, both our experiments and analytical modeling show that the magnetostatic interaction plays an important role in the magnetization reversal process for ferromagnetic submicron dot arrays with small interdot distances. Namely, decreases of vortex nucleation and annihilation fields as well as increase of initial susceptibility occur, accompanied by vortex instability.

This work was supported, in part, by the Korea Institute for Advanced Study, RTF of JSPS, INTAS Grant No. 31-311 and the Grant-in-Aid for Scientific Research from the Ministry of Education, Science and Culture in Japan. Work at ANL was supported by the U.S. Department of Energy, BES Materials Sciences under Contract No. W-31-109-ENG-38.

*Corresponding author. Electronic address: novosad@anl.gov

- ¹M. C. Abraham, H. Schmidt, T. A. Savas, H. I. Smith, C. A. Ross, and R. J. Ram, *J. Appl. Phys.* **89**, 5667 (2001).
- ²M. Grimsditch, Y. Jaccard, and I. K. Schuller, *Phys. Rev. B* **58**, 11 539 (1998).
- ³R. P. Cowburn, A. O. Adeyeye, and M. E. Welland, *New J. Phys.* **1**, 16 (1999).
- ⁴K. Yu. Guslienko, *Appl. Phys. Lett.* **75**, 394 (1999).
- ⁵A. Aharoni, *J. Appl. Phys.* **68**, 2892 (1990).
- ⁶R. P. Cowburn, D. K. Koltsov, A. O. Adeyeye, M. E. Welland, and D. M. Tricker, *Phys. Rev. Lett.* **83**, 1042 (1999).
- ⁷M. Schneider, H. Hoffmann, and J. Zweck, *Appl. Phys. Lett.* **77**, 2909 (2000).
- ⁸A. Fernandez and C. J. Cerjan, *J. Appl. Phys.* **87**, 1395 (2000).
- ⁹T. Shinjo, T. Okuno, R. Hassdorf, K. Shigeto, and T. Ono, *Science* **289**, 5481 (2000).
- ¹⁰R. Pulwey, M. Rahm, J. Biberger, and D. Weiss, *IEEE Trans. Magn.* **37**, 2076 (2001).

- ¹¹N. Kikuchi, S. Okamoto, O. Kitakami, Y. Shimada, S. G. Kim, Y. Otani, and K. Fukamichi, *IEEE Trans. Magn.* **37**, 2082 (2001).
- ¹²J.-G. Zhu, Y. Zheng, and G. Prinz, *J. Appl. Phys.* **87**, 6668 (2000).
- ¹³M. Hanson, C. Johansson, B. Nilsson, P. Isberg, and R. Wäppling, *J. Appl. Phys.* **85**, 2793 (1999).
- ¹⁴M. Schneider and H. Hoffmann, *J. Appl. Phys.* **86**, 4539 (1999).
- ¹⁵A. Lebib, S. P. Li, M. Natali, and Y. Chen, *J. Appl. Phys.* **89**, 3892 (2001).
- ¹⁶V. Novosad, K. Yu. Guslienko, Y. Otani, H. Shima, K. Fukamichi, N. Kikuchi, O. Kitakami, and Y. Shimada, *IEEE Trans. Magn.* **37**, 2088 (2001).
- ¹⁷K. Yu. Guslienko, V. Novosad, Y. Otani, H. Shima, and K. Fukamichi, *Appl. Phys. Lett.* **78**, 3848 (2001).
- ¹⁸N. A. Usov and S. E. Peschany, *Fiz. Met. Metalloved.* **12**, 13 (1994).
- ¹⁹K. Yu. Guslienko, V. Novosad, Y. Otani, H. Shima, and K. Fukamichi, *Phys. Rev. B* (to be published).
- ²⁰K. Yu. Guslienko, *Phys. Lett. A* **278**, 293 (2001).